Wideband Bandstop Filter Based on Capacitively Coupled $\lambda/4$ Short-Circuited Lines

Thai Hoa Duong[1] · Ihn Seok Kim[2]

Abstract

A new wideband bandstop filter(BSF) with a sharp roll-off characteristic is introduced in a stripline structure in this paper. The BSF consists of two sections: the first is two capacitively coupled $\lambda/4$ short-circuited lines with opposite ground positions, while the second is a capacitively coupled $\lambda/4$ short-circuited line. The BSF provides three transmission zeros within the stopband and better than 22 dB rejection over the whole wireless local area network (WLAN) band from 5.15 to 5.825 GHz. The BSF, cascaded to an U.S. ultra-wideband(UWB: 3.1～10.6 GHz) bandpass filter(BPF), is simulated with HFSS and realized with low-temperature co-fired ceramic(LTCC) green tape with a dielectric constant of 7.8. The measurement results agree well with the HFSS simulation results. The size of the UWB BPF including the BSF is $3\times6.3\times0.45$ mm^3.

Key words : Ultra Wideband(UWB), Bandpass Filter(BPF), Wireless Local Area Network(WLAN), Bandstop Filter (BSF), Capacitive Coupling, Capacitively Coupled $\lambda/4$ Short-Circuited Lines, Low-Temperature Co-fired Ceramics(LTCC).

Ⅰ. Introduction

Bandstop filters(BSFs) have provided solutions to prevent RF and microwave circuits and systems from unwanted signals. Thus, a number of studies on BSFs have been published to the present time[1]~[10]. All of the referenced works have used basically uniplanar structures adopting stubs, side coupled lines, and some combination of these two types. Conventional BSFs were designed by using low-pass prototypes with proper frequency transformation[1],[2]. However, the problem of fabricating high impedance lines for the connecting lines of open stubs was an inherent difficulty[3],[4]. Hence, several methods were developed to overcome this problem[5]~[10]. In [5], a wideband BSF with two open-stubs and air bridges was designed with a coplanar waveguide structure, but selectivity was a problem. Ref. [6] presented the design of a wideband BSF using a single open stub and a coupled line. However, the higher passband of the filter deteriorated with loss. A BSF based on a side coupling structure was published; this was geared toward suppressing interference in ultra-wideband(UWB) applications[7]. This work, however, showed very narrow band responses. In [8], a signal interference technique was adopted to design a wideband BSF. The filter had good selectivity, but exhibited only 10 dB return loss at two pass bands. In 2008, two sharp rejection wideband BSFs were developed[9],[10]; here, a BSF based on a loop resonator and three open stubs showed very high selectivity, but high impedance lines were required[9]. In [10], two parallel coupled microstrip line sections in a shunt connection were introduced to design a compact wideband BSF. The measurement results showed good characteristics.

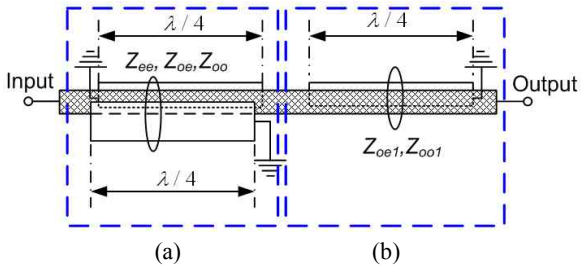

Fig. 1. Proposed bandstop filter structure with a main line (shaded section) and capacitively coupled $\lambda/4$ short-circuited lines (empty sections).

In this paper, a new BSF structure based on capacitively coupled $\lambda/4$ short-circuited lines is introduced for UWB applications in the U.S. We utilize low-temperature co-fired ceramic(LTCC) technology to realize a wideband BSF with 3 dB cutoff frequencies at 4.8 and 6.1 GHz. The BSF has been designed to block the signals at wireless local area network(WLAN) frequencies from 5.15 to 5.825 GHz. Then, the WLAN BSF struc-

Manuscript received June 15, 2010 ; revised August 13, 2010. (ID No. 20100615-018J)
[1]University of Melborn, Australlia.
[2]College of Electronics & Information, Kyung Hee University, Yongin, Korea.
Corresponding Author: Ihn Seok Kim (e-mail : ihnkim@khu.ac.kr)

ture is cascaded to a U.S. UWB bandpass filter(BPF) based on capacitively coupled double T resonators[11]. In Section Ⅱ, an analysis and the design theory for the proposed BSF are presented. For verification, the WLAN BSF structure included in the UWB BPF is simulated with HFSS and realized with LTCC green tape with a dielectric constant of 7.8 in Section Ⅲ. In this section, the measurement and HFSS simulation results are compared.

Ⅱ. Analysis and Design Theory

The proposed BSF structure is shown in Fig. 1. The structure has two sections. The first one, in Fig. 1(a), consists of the main line and two capacitively coupled $\lambda/4$ short-circuited lines, one above and the other below the main line; here, Z_{ee}, Z_{oe}, and Z_{oo} are the mode impedances with respect to EE-mode, OE-mode, and OO-mode, as discussed in [12]. The second section, in Fig. 1(b), comprises the main line with a capacitively coupled $\lambda/4$ short-circuited line, where Z_{oe1} and Z_{oo1} are the even and odd mode characteristic impedances of the second coupled line. The positions of the ground points for the two coupled short-circuited $\lambda/4$ lines in the first section should be in opposite directions.

2-1 The Two Capacitively Coupled $\lambda/4$ Lines in the First Section

As shown in Fig. 2(a), the relationship of the port voltages and currents for the three-line structure can be expressed by:

$$[V]=[Z_{6\times6}][I] \tag{1}$$

where $[V]$ and $[I]$ are 6×1 column matrices and $[Z_{6\times6}]$ is the 6×6 impedance matrix, which can be obtained in terms of the normal modes of the coupled three-line structure as in [12] and [13].

The two capacitively coupled $\lambda/4$ lines with the main line in Fig. 2(b) can be treated as a two-port network from the expression for the six-port network in Fig. 2(a), with the following conditions:

$$V_1 = V_4 = 0 \tag{2}$$

$$I_3 = I_6 = 0 \tag{3}$$

$$I_i = I_2 \tag{4}$$

$$I_o = I_5 \tag{5}$$

$$V_i = V_2 \tag{6}$$

$$V_o = V_5 \tag{7}$$

$$\begin{bmatrix} V_i \\ V_o \end{bmatrix} = [Z_A] \begin{bmatrix} I_i \\ I_o \end{bmatrix} \tag{8}$$

$$S_{11}^A = \frac{(Z_{11}^A - Z_0)(Z_{22}^A + Z_0) - Z_{12}^A Z_{21}^A}{(Z_{11}^A + Z_0)(Z_{22}^A + Z_0) - Z_{12}^A Z_{21}^A}$$

$$S_{12}^A = \frac{2Z_{12}^A Z_0}{(Z_{11}^A + Z_0)(Z_{22}^A + Z_0) - Z_{12}^A Z_{21}^A}$$

$$S_{21}^A = \frac{2Z_{21}^A Z_0}{(Z_{11}^A + Z_0)(Z_{22}^A + Z_0) - Z_{12}^A Z_{21}^A}$$

$$S_{22}^A = \frac{(Z_{11}^A + Z_0)(Z_{22}^A - Z_0) - Z_{12}^A Z_{21}^A}{(Z_{11}^A + Z_0)(Z_{22}^A + Z_0) - Z_{12}^A Z_{21}^A} \tag{9}$$

By substituting (2)~(7) into (1), the impedance matrix $[Z_A]$ in (8) for the network in Fig. 2(b) can be determined. Then, the S-parameter ($[S^A]$) for the structure in Fig. 1(a) can be extracted as (9)[14]. The two coupled short-circuited lines in the first section provide two transmission zeros that are symmetric at the center frequency within the stopband, as shown in Fig. 3. However, $|S_{21}|$ is almost better than 10 dB within the rejection band.

The bandwidth of the structure in Fig. 1(a) can be controlled by the coupling between the main line and the $\lambda/4$ short-circuited line, C_A, where C_A is the coupling coefficient between the main line and the $\lambda/4$ short-circuited line. In order to demonstrate the bandwidth property of the short-circuited coupled line structure in the first section, Fig. 4 shows the $|S_{11}|$ characteristics of the proposed structure depending on the coupling coefficient C_A=6.9~15.6 dB. The higher the C_A, the wider the bandwidth of the stopband. The structure can provide wider stopband characteristics with a smaller coupling C_A.

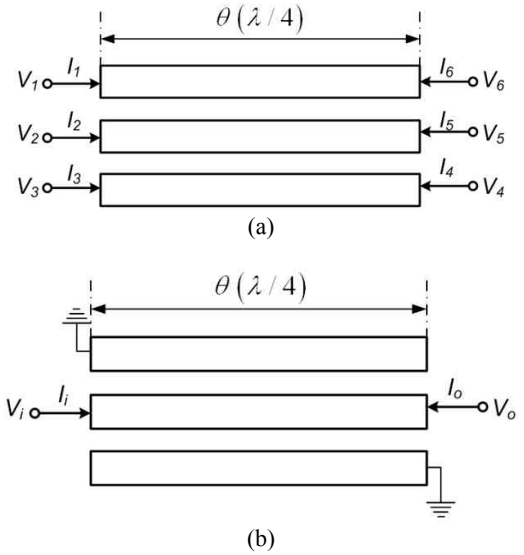

Fig. 2. (a) A general six-port three-line structure. (b) A two-port network simplified from two capacitively coupled $\lambda/4$ short-circuited lines in the first section.

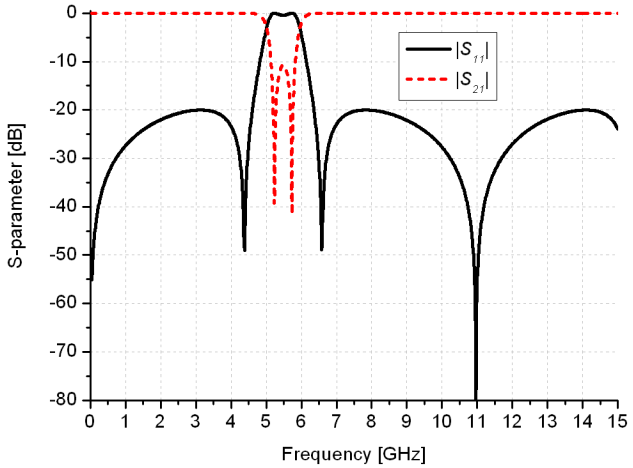

Fig. 3. Frequency response for the two $\lambda/4$ capacitively short-circuited coupled lines of the first section.

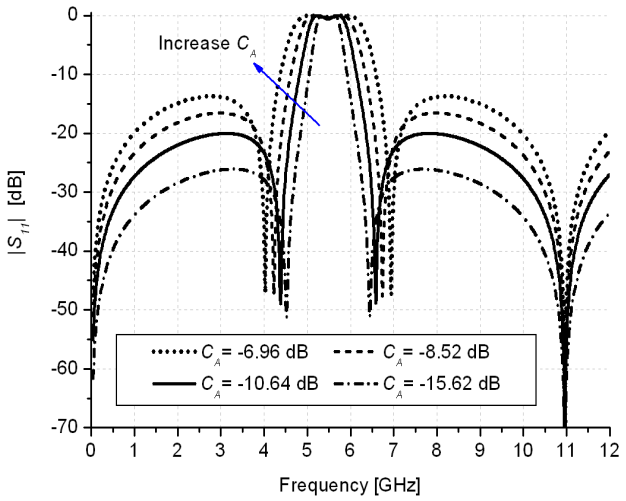

Fig. 4. Bandwidth property depending on the coupling coefficient between the main line and the two $\lambda/4$ short-circuited lines in the first section.

2-2 The Capacitively Coupled $\lambda/4$ Line in the Second Section

The structure of the capacitively coupled $\lambda/4$ short-circuited line in the second section is shown in Fig. 1(b), and its impedance matrix ($[Z_B]$) can be calculated by

$$[Z_B]=\begin{bmatrix} j\dfrac{Z_{1-}^2-Z_{1+}^2\cos^2\theta}{Z_{1+}\sin 2\theta} & j\dfrac{Z_{1-}^2-Z_{1+}^2}{2Z_{1+}\sin\theta} \\ j\dfrac{Z_{1-}^2-Z_{1+}^2}{2Z_{1+}\sin\theta} & j\dfrac{Z_{1-}^2-Z_{1+}^2}{2Z_{1+}\tan\theta} \end{bmatrix}, \tag{10}$$

where $Z_{1+}=Z_{oe1}+Z_{oo1}$, $Z_{1-}=Z_{oe1}-Z_{oo1}$, and Z_{oe1} and Z_{oo1} are the even- and odd-mode characteristic impedances of the coupled line structure, respectively. The coupled short-circuited line is an odd-mode resonator. Therefore, we have designed a coupled line resonant at the center frequency of the stopband(5.49 GHz), as shown in Fig. 5. The S-parameter ($[S^B]$) of the coupled line was calculated in a similar way to (9)[14]. This characteristic has been used to improve the rejection property of the short-circuited coupled line structure in the first section.

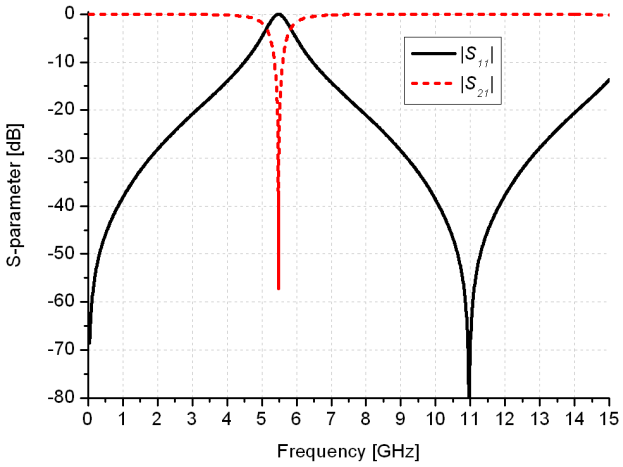

Fig. 5. Frequency response for the $\lambda/4$ capacitively coupled short-circuited line in the second section.

2-3 WLAN Bandstop Filter

By cascading the two BSF structures, one more transmission zero at the center frequency of the second coupled structure has been added to the stopband in Fig. 3. The S-parameters of the cascaded structure ($[S^{cascade}]$) have been calculated as (11)~(14)[15], where $[S^A]$ and $[S^B]$ are the S-parameters of the first and second coupled line structures, respectively. As shown in Fig. 6, a very sharp roll-off stopband frequency response and higher rejection with three transmission zeros have been obtained. $|S_{21}|$ is less than -27 dB within the stopband and the return loss better than 20 dB in the two pass bands up to 15 GHz. Because of the odd-mode property of the short-circuited resonator, the stopband harmonics repeat every $2f_o$, where f_o=5.49 GHz is the center frequency of the stopband:

$$S_{11}^{cascade}=S_{11}^{A}+\frac{S_{12}^{A}S_{11}^{B}S_{21}^{A}}{1-S_{22}^{A}S_{11}^{B}} \tag{11}$$

$$S_{12}^{cascade}=\frac{S_{12}^{A}S_{12}^{B}}{1-S_{22}^{A}S_{11}^{B}} \tag{12}$$

$$S_{21}^{cascade}=\frac{S_{21}^{A}S_{21}^{B}}{1-S_{22}^{A}S_{11}^{B}} \tag{13}$$

$$S_{22}^{cascade}=S_{22}^{B}+\frac{S_{21}^{B}S_{11}^{A}S_{12}^{B}}{1-S_{22}^{A}S_{11}^{B}} \tag{14}$$

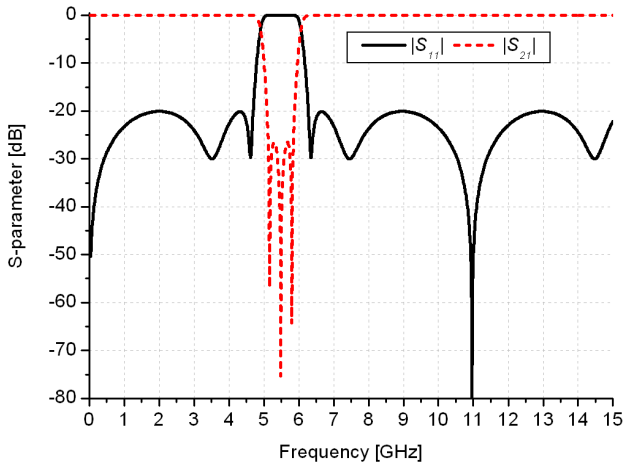

Fig. 6. Frequency response of the proposed BSF for WLAN stopband application.

Ⅲ. WLAN Stopband Included in UWB

The proposed BSF structure has been added at the output port of the capacitively coupled double T resonator UWB BPF(3.1～10.6 GHz) in [11], as shown in the dotted box in Fig. 7(b). The double T resonator UWB BPF has been rearranged to obtain a compact size of 3×6.3 mm^2. The structure consists of 10 layers and each layer has a thickness of 43 μm and a dielectric constant of 7.8. The UWB BPF circuits are located on the fourth, fifth, and sixth layers, and the three layers of the WLAN BSF structure are located on the third, fifth, and seventh layers, respectively, to obtain the required bandwidth for the stopband. Via walls are added to the structure instead of solid walls in order to reduce the effects of interference between stripline structures.

To obtain a good bandstop property, as shown in Fig. 6, the coupling coefficient between the main line and the lower $\lambda/4$ short-circuited line in the first section and that in the second section should be identical. Therefore, w_{1l}=w_2=0.08 mm and off_{1l}=off_2=0.05 mm have been chosen, as shown in Fig. 7. In addition, in order to meet the bandwidth of the BSF, the coupling coefficient between the main line and the upper $\lambda/4$ short-circuited line in the first section has been selected as −10.64 dB in Fig. 4. Hence, w_{1u}=0.15 mm and off_{1u}=0.08 mm have been chosen. Fig. 8 shows the HFSS simulation result for the proposed BSF. The insertion loss within the stopband from 5.15 to 5.825 is better than 22 dB and the return loss less than 15 dB at 1 GHz from the edges of the stopband.

Fig. 9 shows the HFSS frequency response for the UWB BPF[11] without the BSF. The filter has a bandwidth from 3.1 to 10.6 GHz and a return loss better than 15 dB. The structure in Fig. 7 has been simulated

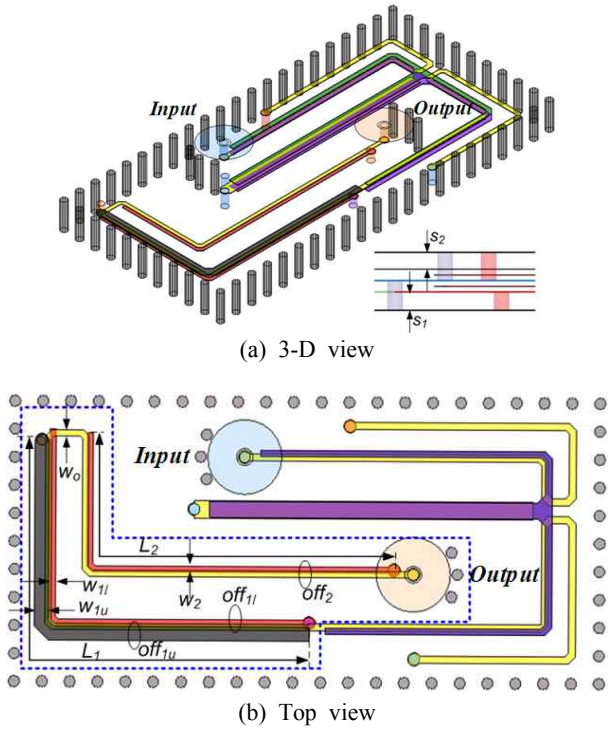

Fig. 7. The structure of the UWB BPF with the WLAN stopband(W_0=0.08 mm, W_{1l}=0.08 mm, W_{1u}=0.15 mm, L_1=4.85 mm, off_{1l}=0.05 mm, off_{1u}=0.07 mm, W_2=0.08 mm, L_2=4.85 mm, off_2=0.05 mm, s_1=s_2=0.129 mm).

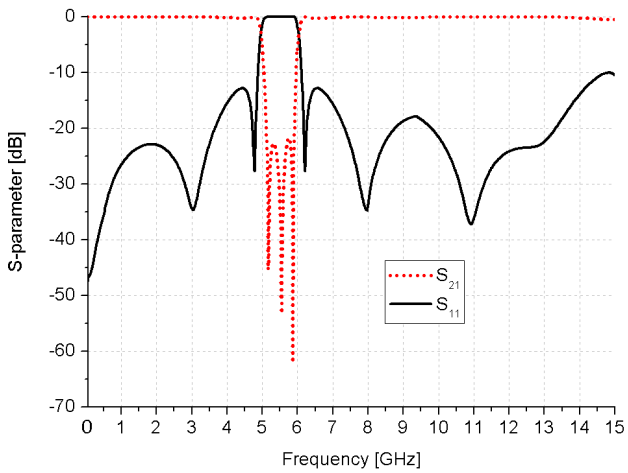

Fig. 8. HFSS frequency response for the proposed bandstop structure shown in the dotted box in Fig. 7.

and tuned with HFSS(v.11, Ansoft), then measured with the Anritsu ME7808A network analyzer and the Cascade Microtech Summit 12971B probe station. Input/output striplines were connected to input/output circular ports with inner and outer diameters of 200 μm and 750 μm, respectively, by solid vias(with a via diameter of 120 μm). Measurement probes with a 400 μm pitch

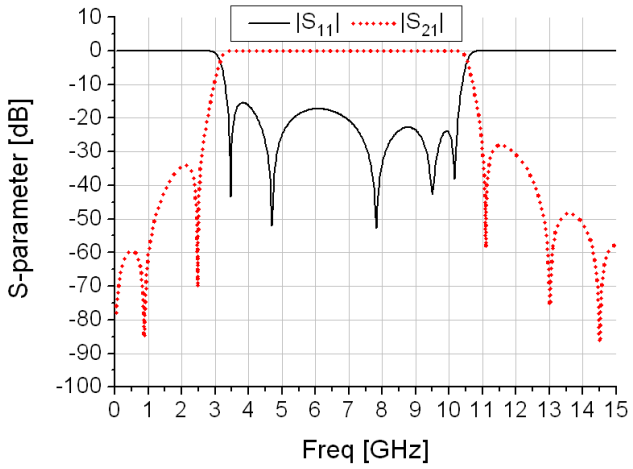

Fig. 9. HFSS frequency response for the UWB BPF using a capacitively coupled double T resonator without a bandstop filter.

size were used to test the filter. Fig. 10 shows the comparisons between the simulation and measurement results for the UWB BPF with a WLAN stopband structure. The dotted line indicates the simulation results and the solid line the measurement results. The simulation results show a dual band from 3.1 to 4.8 GHz and 6.1 to 10.6 GHz. $|S_{21}|$ is better than 22 dB within the stopband and the return loss better than 12 dB for the two passbands. An insertion loss less than 0.8 dB for the passbands and a rejection better than 22 dB within the stopband from 5.15 to 5.825 GHz have been measured. The proposed WLAN BSF has sharp roll-off characteristics. The attenuation slope in the lower transition region(~4.8 GHz) is 90 dB/GHz and the slope in the upper transition region(~6.1 GHz) is 83 dB/GHz. The

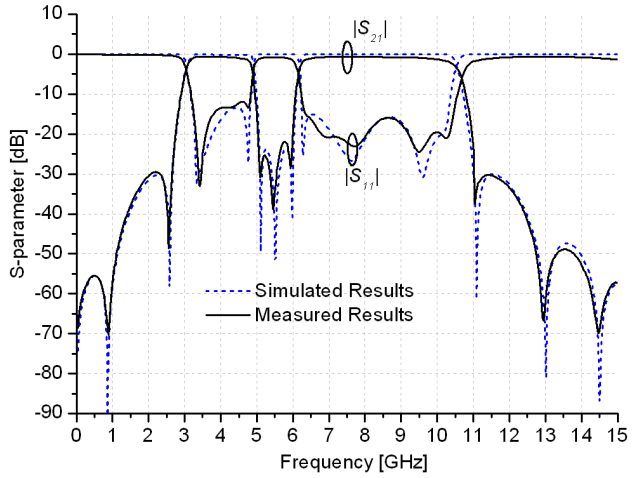

Fig. 10. Comparison between the simulated and measured results for the UWB BPF with the 5 GHz WLAN stopband.

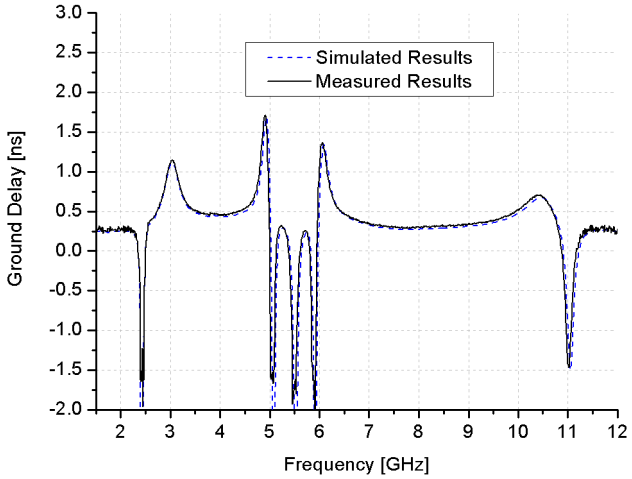

Fig. 11. Group delay characteristics for the UWB BPF with WLAN BSF.

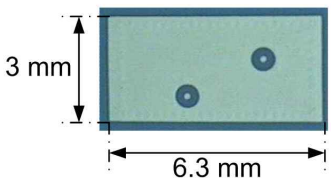

Fig. 12. Top view of the fabricated UWB BPF with the WLAN stopband.

size of the UWB BPF with WLAN BSF is 3×6.3×0.45 mm^3. Fig. 11 shows the group delay property of the structure in Fig. 7. The measured group delay is less than 0.7 ns within the two passbands. Group delays at the centers of the first and second passbands are 0.49 ns and 0.31 ns, respectively. Fig. 12 shows the top views of the fabricated UWB BPF with the WLAN stopband.

Ⅳ. Conclusion

In this paper, we introduced a wideband sharp rejection BSF based on capacitively coupled $\lambda/4$ short-circuited lines in LTCC technology. The rejection bandwidth can be varied by changing the capacitive coupling between the main line and the $\lambda/4$ short-circuited lines. By cascading two capacitively coupled $\lambda/4$ short-circuited lines with opposite ground positions and a capacitively coupled $\lambda/4$ short-circuited line, three transmission zeros with high rejection and good out-of-band characteristics have been achieved. The wideband BSF structure has been inserted into a UWB BPF based on a double T resonator structure[11]. The measurement results agree well with simulation results. We expect that the sharp roll-off characteristics and compact structure of the BSF make it very suitable to protect WLAN,

worldwide interoperability for microwave access(Wi-MAX), and industrial scientific medical(ISM) signals for UWB applications.

The authors wish to acknowledge the financial support of LG Innotek and the measurement assistance of the KETI(Korea Electronics Technology Institute).

References

[1] G. Matthaei, L. Young, and E. M. T. Jones, *Microwave Filters, Impedance Matching Networks, and Coupling Structures*, Chapter 4, pp. 83-162, Boston, MA: Artech House, 1980.

[2] L. Young, G. Matthaei, and E. M. T. Jones, "Microwave bandstop filters with narrow stopbands", *IRE Trans. Microwave Theory Tech*., vol. MTT-10, no. 11, pp. 416-427, Nov. 1962.

[3] B. Schiffman, G. Matthaei, "Exact design of bandstop microwave filters", *IEEE Trans. Microwave Theory Tech*., vol. MTT-12, no. 1, pp. 6-15, Jan. 1964.

[4] M. Horton, R. Menzel, "General theory and design of optimum quarter wave TEM filters", *IEEE Trans. Microwave Theory Tech*., vol. MTT-13, no. 3, pp. 316-327, May 1965.

[5] H. A. Gorur, C. Karpuz, "Uniplanar compact wideband bandstop filter", *IEEE Microwave Wireless Compon. Lett*., vol. 13, no. 3, pp. 114-116, Mar. 2003.

[6] M. Hsieh, S. Wang, "Compact and wideband microstrip bandstop filter", *IEEE Microwave Wireless Compon. Lett*., vol. 15, no. 7, pp. 472-474, Jul. 2005.

[7] K. Rambabu, M. Y.-W. Chia, K. M. Chan, and J. Bornemann, "Design of multiple-stopband filters for interference suppression in UWB applications", *IEEE Trans. Microwave Theory Tech*., vol. MTT- 25, no. 8, pp. 3333-3338, Aug. 2006.

[8] J. K. Mandal, S. Sanyal, "Compact bandstop filter using signal interference technique", *Electron. Lett*., vol. 43, no. 2, pp. 110-111, Jan. 2007.

[9] K. Divyabramham, M. K. Mandal, and S. Sanyal, "Sharp-rejection wideband bandstop filter", *IEEE Microwave Wireless Compon. Lett*., vol. 18, no. 10, pp. 662-664, Oct. 2008.

[10] M. K. Mandal, K. Divyabramham, and S. Sanyal, "Compact, wideband bandstop filters with sharp rejection characteristic", *IEEE Microwave Wireless Compon. Lett*., vol. 18, no. 10, pp. 665-667, Oct. 2008.

[11] T. H. Duong, I. S. Kim, "New elliptic function type UWB BPF based on capacitively coupled $\lambda/4$ open T resonator", *IEEE Trans. Microwave Theory Tech*., vol. MTT-57, no. 12, pp. 3089-3098, Dec. 2009.

[12] D. Pavlidis, H. L. Hartnagel, "The design and performance of three-line microstrip couplers", *IEEE Trans. Microwave Theory Tech*., vol. MTT-24, no. 10, pp. 631-640, Oct. 1976.

[13] V. K. Tripathi, "On the analysis of symmetrical three-line microstrip circuits", *IEEE Trans. Microwave Theory Tech*., vol. MTT-25, no. 9, pp. 726-729, Sep. 1977.

[14] D. M. Pozar, *Microwave Engineering*, Chapter 4, p. 187, 2nd Ed., New York: John Wiley, 1998.

[15] R. J. Cameron, C. M. Kudsia, and R. R. Mansour, *Microwave Filters for Communication Systems*, p. 123, New Jersey: John Wiley, 2007.

Thai Hoa Duong

was born in HCM City, Vietnam in 1981. He received the B.S. degree in electrical engineering from Ho Chi Minh City University of Technology, Vietnam in 2004 and his Ph.D. degree in Radio Engineering from the Kyung Hee University, South Korea, in 2010. His research interests include the design, analysis, synthesis, and miniaturization of microwave planar ultra wideband passive devices, such as bandpass filters, power divider/combiners, and directional couplers for wireless communication systems. He served as a reviewer for IEEE MTT and MWCL from Feb. 2010 to the present.

Ihn Seok Kim

received his B.E. degree in electrical engineering from Kyung Hee University in 1974 and his M.Sc. and Ph.D. degrees in electrical engineering from the University of Ottawa, Canada, in 1983 and 1991, respectively. From 1973 to 1992, he had worked at Korean Broadcasting Systems as an RF engineer, at Com Dev as technical staff, General Instrument of Canada as a senior engineer, the Canadian Space Agency as a research scientist, and the Korean Mobile Telecommunications Corporation as a senior researcher. In 1992, he joined Kyung Hee University, where he has been working on the modeling of various microwave structures, their applications to filters, power divider/combiners, and microwave oscillators. He also works in the EMI/C field as a member of the Korean delegation for the CISPR B/F and TC 77C committees. From February 1999 to February 2000, he was on sabbatical at ETH(Zurich) and the Motorola EM Lab.(Ft. Lauderdale). He served as a reviewer for IEEE Microwave Theory and Techniques Society from 1998 to the present.